# DISENTANGLING UP AND DOWN FLOW CHARACTERISTICS OF A TURBULENT NUCLEAR FLUIDISED BED BY AUTO-REGRESSIVE MODELING OF GAMMA-TRANSMISSION FLUCTUATIONS

T.H.J.J. van der Hagen[*], W. Harteveld, R.F. Mudde and S. Verdoold
Kramers Laboratorium voor Fysische Technologie
Delft University of Technology
Prins Bernhardlaan 6, 2628 BW Delft, The Netherlands
hagen@iri.tudelft.nl ; r.f.mudde@klft.tn.tudelft.nl

[*]also: Interfaculty Reactor Institute
Delft University of Technology
Mekelweg 15, 2629 JB Delft, The Netherlands

## ABSTRACT

The combination of rising bubbles and falling particle clusters in a fluidized bed yields an interference pattern in the *CCF* and in the *CPSD*-phase of the signals of two axially displaced gamma-source/detector sets. Bivariate autoregressive modeling can disentangle these two processes and yields velocity estimates and additional information on physical properties for both. The technique developed here is another example of the power of noise analysis for nuclear-engineering studies.

## 1. INTRODUCTION

Delft University of Technology is presently studying the basic concept of a modular fluidized bed nuclear fission reactor, FLUBER. FLUBER consists of a graphite cylinder, partly filled with coated fuel particles (1-mm diameter).[1] Earlier studies have indicated that in a well-designed system – with a sufficiently undermoderated collapsed core – reactivity can be increased until criticality is reached by fluidizing the particles on a helium flow, which transports the fission heat to a gas turbine. In absence of coolant flow, the particles fall back at the bottom of the bed, yielding a strongly subcritical reactor. This aspect guarantees inherent safety as to reactivity transients.
A bed expansion of about a factor three is necessary to induce a large enough reactivity swing. Such an expansion calls for high coolant velocities that lead to a fluidized bed operating in the turbulent flow regime. This regime has excellent mixing characteristics, but shows strong space

dependent gas-fraction fluctuations, which influence the neutronic behavior of the system.

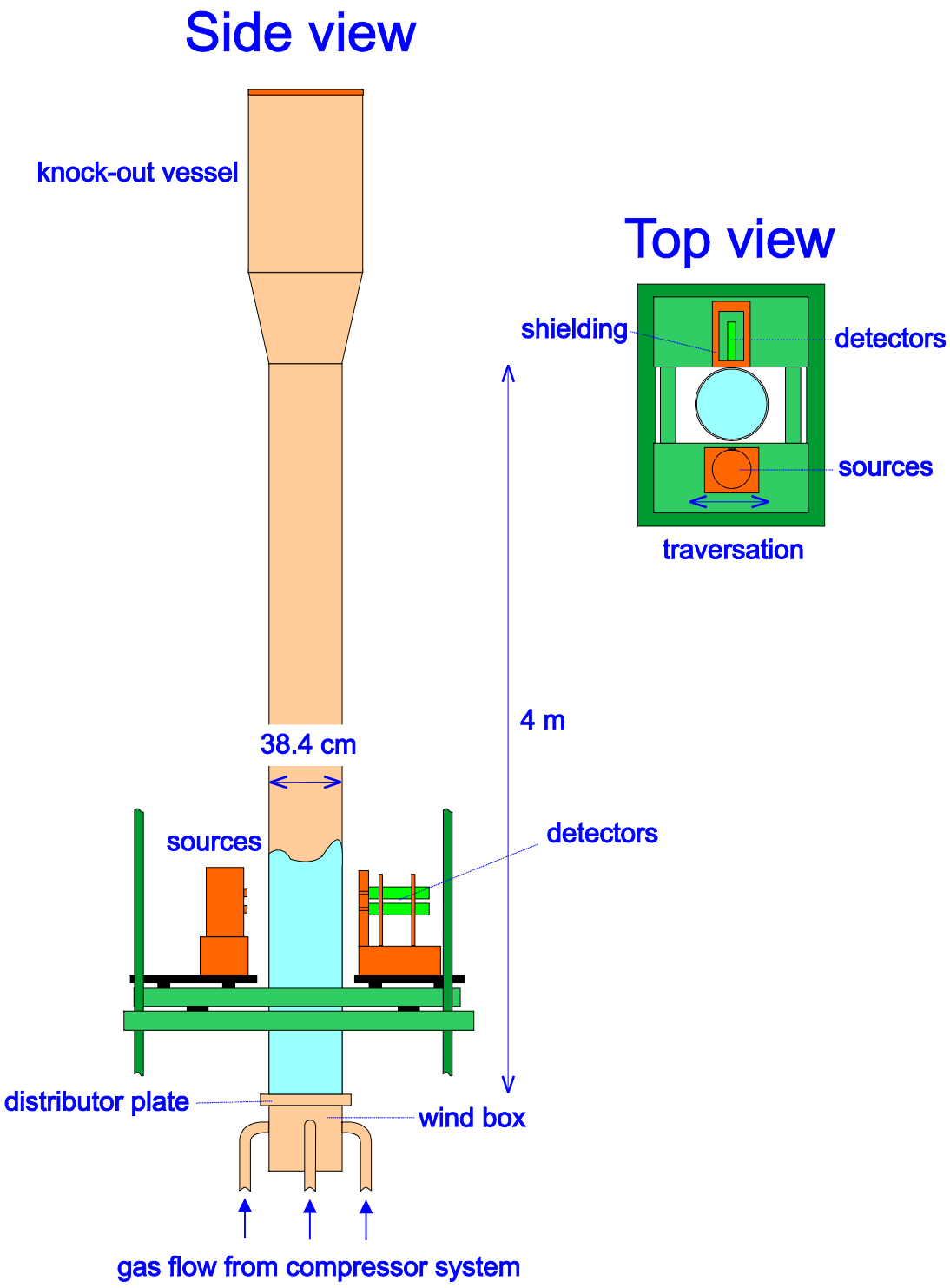


Figure 1. Fluidized bed experimental set-up.

Fluidization aspects were investigated by measurements on a test facility operating at ambient conditions.[6] Here, polystyrene particles and air were used as system models. The facility used consists of a 4-meter tall, 38-cm inner diameter column (see Fig. 1). Gas-fraction profiles were measured using the attenuation of a collimated gamma beam. To this end, a 100-mCi $^{137}$Cs source – emitting 662-keV gammas – and a BGO-detector were positioned at opposite sides of the facility.

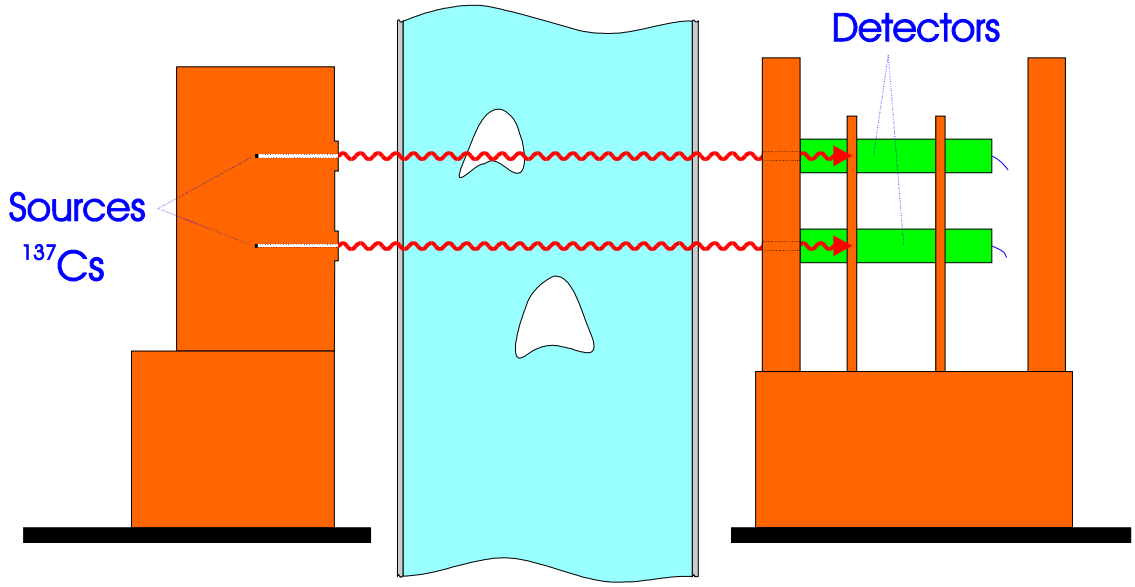


Figure 2. Gamma-transmission set-up for velocity measurements consisting of two gamma beams and two detectors.

Particle-cluster and 'bubble' velocities were measured by using *two* of these gamma-source/detector sets, by correlating the signals of two – axially displaced – gamma sensors. Figure 2 illustrates this technique. Such a correlation technique is commonly used in industrial and experimental set-ups for determining transit times of fluctuations from one sensor to the other, where the transit time manifests itself as the slope of the linear phase spectrum of the cross power spectral density (*CPSD*). In our case, however, quite different results were obtained, due to the fact that the fluidized bed is not a pure transit-time system. The combination of rising bubbles and particles (especially through the center of the bed) with falling particle clusters (mainly along the periphery) yields a strong distortion of the phase of the *CPSD* of the two gamma-transmission signals.

The challenge of the work presented here is to extract information on both the up and down flows from the measured time series. The problem is especially hard to solve because the two physical processes both have a broad frequency content; they both influence the *CPSD* over a wide range of frequencies.

## 2. CROSS-CORRELATION FUNCTIONS

Figure 3 displays the cross-correlation functions (*CCF*s) for a measurement where the gamma beams were radiating through the center of the bed (left figure) and through the periphery of the bed (right figure). Two distinct peaks, that would correspond to an up and a down flow, cannot be seen in these functions. The *CCF*s could be optimized for delay-time estimation by using the Hannan-Thomson weighting function in the frequency domain.[5] In this manner, the time resolution of the *CCF*s is strongly improved, but the amplitudes of the functions are corrupted, which is the reason for the use of numberless linear vertical axes in Figs. 3. At a radial position near the periphery of the column a peak at negative time delay – corresponding to downward flowing processes – and a peak at a positive time delay – corresponding to upward flowing processes – can now clearly be seen. Apparently, up-flowing processes are strongly dominating in the center of the bed, since the corresponding *CCF* yields only a peak at a positive time delay. Although the improvement is substantial, still, the interference of the two peaks (due to overlap) hampers a complete separation of the two processes and a correct estimate of the individual velocities.

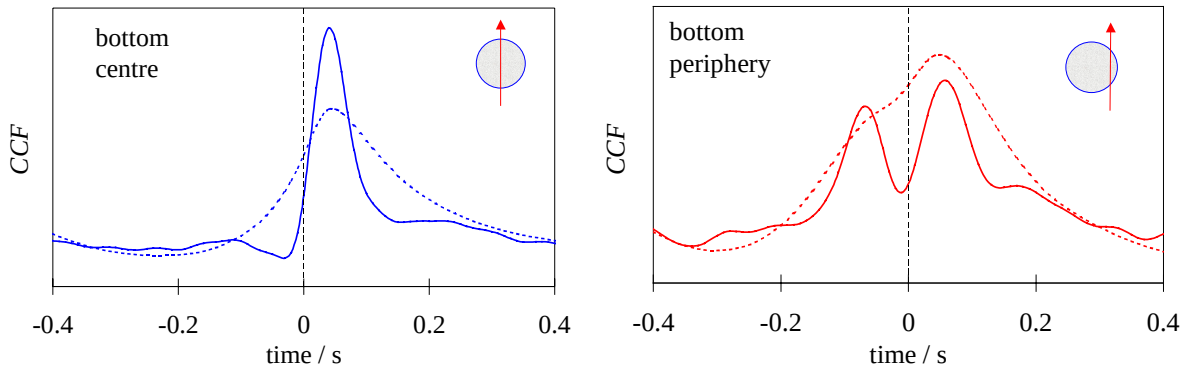


Figure 3. Cross-correlation functions (*CCF*s) of measured gamma-transmission signals, using standard (dashed lines) and Hannan-Thomson weighted (solid lines) correlation techniques. Left: radiating through the bed center; right: radiating through the bed periphery.

The essence of the problem and a route to solve it will become clear after we have described the characteristic functions to be expected in mathematical terms, by using a simplified model. This is done in the next section.

## 3. INSIGHT BY A SIMPLE MODEL

Many researchers in reactor physics have contributed to a better understanding of the so-called local-global problem. Here, the challenge was to explain and use the signals of two axially displaced in-core neutron detectors, where an interference between global, reactivity induced, neutron flux fluctuations, and local signal perturbations, mainly induced by traveling steam

bubbles, led to complicated characteristic functions, such as, coherence and phase and amplitude of the cross-power spectral density. The proceedings of the SMORN-meetings (Specialists' Meetings on Reactor Noise) contain many valuable papers on this topic. Also, the review paper by Stekelenburg and Van der Hagen (1993) might be helpful as a starting point for the interested reader.[8]
In the local-global case, there is a distinct separation in phase and in frequency of the two processes: global fluctuations are indeed global, they are 'felt' by all detectors at the same time, i.e. without time delay, whereas the passing bubbles perturb the detector signals one after another, just like the situation in the fluidized bed. Global perturbations contain only low-frequency components (below a few hertz), whereas the bubbles influence the spectra up to some 50 Hz. These two facts made a separation relatively easy.

In the present case, the situation is more complicated: both processes (up-flowing and down-flowing 'sources of signal fluctuations') are likely to have more or less the same frequency content; both processes induce a time delay (a positive and a negative respectively) between the two detector signals.
We will use a simple analytical model to calculate the characteristic functions to be expected. In this model, the fluctuating part of the signal of the lower gamma detector ($\delta S_1$) is composed of an up-flowing component, $u(t)$ (that is assumed to arrive undistorted at the upper detector position after a time $\tau_1$), a component that is due to noise flowing downward and an intrinsic (purely local) noise source, $\varepsilon_1(t)$. In a similar manner, the fluctuating part of the signal of the upper gamma detector ($\delta S_2$) is composed of a down-flowing component, $d(t)$ (that is assumed to arrive undistorted at the lower detector position after a time $\tau_2$), a component that is due to noise flowing upward and an intrinsic noise, $\varepsilon_2(t)$:

$$\begin{aligned} \delta S_1(t) &= u(t) + d(t-\tau_2) + \varepsilon_1(t); \\ \delta S_2(t) &= u(t-\tau_1) + d(t) + \varepsilon_2(t). \end{aligned} \tag{1}$$

The correlation function of these two signals can easily be calculated if it is assumed that the noise sources, $u$, $d$, $\varepsilon_1$ and $\varepsilon_2$ are uncorrelated. The result is (for simplicity, we use non-normalized correlation functions here):

$$CCF(t) = <\delta S_1(t')\cdot\delta S_2(t'+t)> = <u(t')\cdot u(t'-\tau_1+t)> + <d(t'-\tau_2)\cdot d(t'+t)>, \tag{2}$$

where $<x>$ denotes the time average of $x$.
The two terms on the right-hand side of this description are equal to the time-shifted auto-correlation functions (*ACF*s) of the two travelling noise sources:

$$CCF(t) = ACF_u(t-\tau_1) + ACF_d(t+\tau_2). \tag{3}$$

As expected, these two components have their maxima at $t=\tau_1$ and $t=-\tau_2$, respectively, leading to two maxima of the *CCF*, provided that their relative contribution to the *CCF* is strong enough.
The *CPSD* of the signals can be found by Fourier transforming the *CCF*:

$$CPSD(f) = \int_{-\infty}^{\infty} CCF(t)\exp(-j2\pi ft)dt =$$

$$= \int_{-\infty}^{\infty} \left(ACF_u(t-\tau_1)\exp(-j2\pi ft) + ACF_d(t+\tau_2)\exp(-j2\pi ft)\right)dt = \quad (4)$$

$$= APSD_u \exp(-j2\pi f\tau_1) + APSD_d \exp(j2\pi f\tau_2),$$

where $j$ is the imaginary unit, $f$ is the frequency (Hz) and where $APSD_u$ and $APSD_d$ are the auto-power spectral densities of the up-flowing and down-flowing noise sources, respectively, which are real functions. The complex nature of the *CPSD* is due to the two time delays, as expressed by the two exponential functions.
The modulus and the phase of the *CPSD* can be expressed more easily if we define $k$ as the relative strength of up-flowing perturbations:

$$k(f) \equiv \frac{APSD_u(f)}{APSD_d(f)}. \quad (5)$$

Note that $k$ is a function of frequency, since the relative importance of the noise sources depends on the frequency. In this simple analysis, however, we will assume $k$ to be constant for all frequencies.
After some algebra, the modulus and phase of the *CPSD* can now be written as:

$$|CPSD(f)| = APSD_u(f)\sqrt{1+\frac{1}{k^2}+\frac{2}{k}\cos(2\pi f(\tau_1+\tau_2))}\,; \quad (6)$$

$$phase(CPSD(f)) = -2\pi f\tau_1 + \tan^{-1}\left(\frac{\sin(2\pi f(\tau_1+\tau_2))}{k+\cos(2\pi f(\tau_1+\tau_2))}\right), \quad for\ k>1; \quad (7)$$

$$phase(CPSD(f)) = 2\pi f\tau_2 - \tan^{-1}\left(\frac{\sin(2\pi f(\tau_1+\tau_2))}{\frac{1}{k}+\cos(2\pi f(\tau_1+\tau_2))}\right), \quad for\ k<1. \quad (8)$$

These equations show that the existence of two noise sources leads to a perturbation of both modulus and phase behavior. From Eq. (6) it can be noticed that the *CPSD* exhibits minima at some specific frequencies, which are equal to:

$$f_{CPSD-minimum} = \frac{1}{2(\tau_1+\tau_2)}, \frac{3}{2(\tau_1+\tau_2)}, \frac{5}{2(\tau_1+\tau_2)} \ldots \quad (9)$$

These minima are equal to $APSD_u\,|1-1/k|$ and are thus equal to zero for $k=1$.

Equations (7) and (8) show that the linear phase behavior that one would obtain for a process with a single time delay is distorted as well. If the up-flowing process is dominant ($k>1$), the linear phase with negative slope $-\tau_1$ is distorted by the tangential interference term in Eq. (7); in cases where the down-flowing process dominates ($k<1$), the phase with positive slope $\tau_2$ is distorted (see Eq.(8)). The phase distortion is zero at the frequencies where the modulus has an extreme:

$$f_{no\ phase\ distortion} = f_{CPSD-extreme} = \frac{1}{2(\tau_1+\tau_2)}, \frac{2}{2(\tau_1+\tau_2)}, \frac{3}{2(\tau_1+\tau_2)} \ldots \qquad (10)$$

Figures 4-7 present some examples of phase and modulus spectra, calculated from Eqs. (6-8). The delay times were chosen (rather arbitrarily) to be 200 and 300 ms.

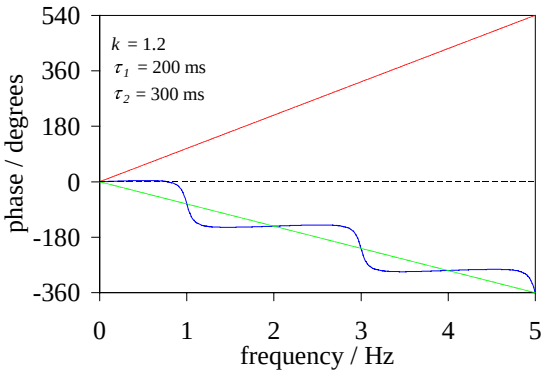


Figure 4. Phase of the *CPSD* when the positive–delay process is stronger ($k>1$), calculated from an analytical model. Blue: two delay-time process; green: positive delay, red: negative delay.

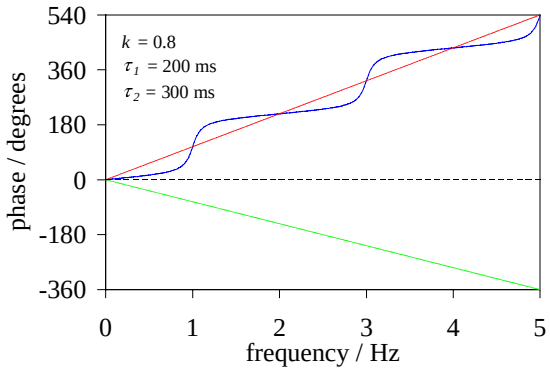


Figure 5. Phase of the *CPSD* when the negative–delay process is stronger ($k<1$), calculated from an analytical model. Blue: two delay-time process; green: positive delay, red: negative delay.

Figure 4 gives the phase spectrum in the case where the up-flowing process is dominant: $k=1.2$. Clearly, the phase (in blue) wags around the slope that would correspond to a pure up-flowing process (in green). When the down-flowing process is the strongest ($k=0.8$, Fig. 5), the phase oscillates around the slope that would correspond to a pure down-flowing process (in red). Fig. 6 shows the dips in the modulus of *CPSD* at the characteristic frequencies (1, 3, 5 … Hz, see Eq. (9)) together with the phase distortion.

For such a system, where $k$ is constant, both delay times can easily be extracted from the phase of the *CPSD* of measured noise signals: the 'average' slope gives the transit time of the dominant noise source; the crossings of the measured phase with the line corresponding to this delay time yields the second delay time via Eq. (10).

An example of the influence of the frequency dependence of $k$ is shown in Fig. 7. Here, $k$ was taken as the frequency value in Hertz divided by 3 Hz (k=f/3). So, the down-flowing process dominates below 3 Hz, the up-flowing process dominates for higher frequencies. As expected, the phase starts off following the linear phase corresponding to the down-flow delay, with increasing distortion as f increases, until 3 Hz where it jumps to the slope of the up-flow process

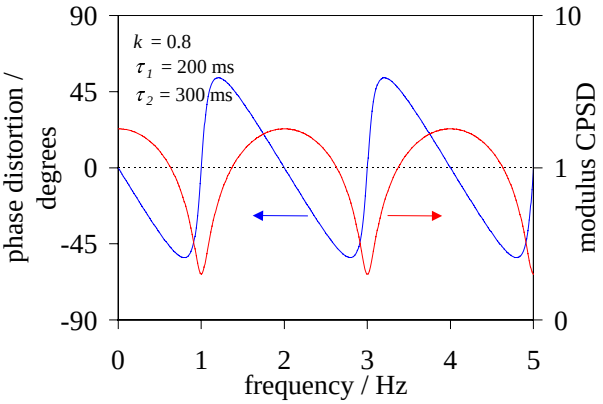


Figure 6. Phase distortion and modulus of the *CPSD* when the negative–delay process is stronger ($k$<1), calculated from an analytical model.

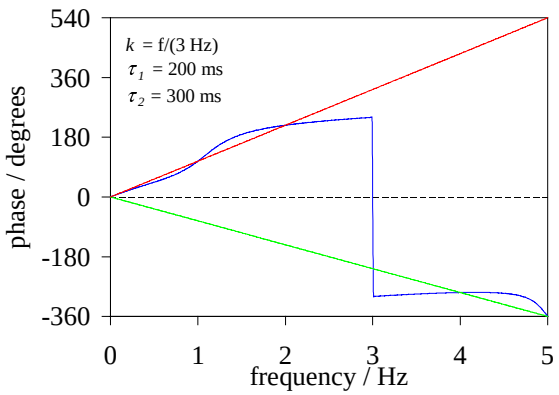


Figure 7. Phase of the *CPSD* when the relative noise strength is frequency dependent ($k(f)$). Here, $k$ is taken as f/(3 Hz).
Blue: two delay-time process;
green: positive delay, red: negative delay.

and continues around this line (the phase spectrum was corrected for jumps of 360 degrees). This picture indicates how complex a measured phase spectrum might be, especially when the dominance of the two noise sources is not nicely separated in the frequency domain.

## 4. BIVARIATE AUTO-REGRESSIVE MODEL

The fact that in our case there is a clear cause-effect relation between the signal perturbations – first the lower signal is affected, thereafter the upper signal, and visa versa – offers good prospects for applying bivariate autoregressive modeling (BAR, see textbooks like the one by Priestley, 1994 for details about this method)[7]. In the traditional local-global case this modeling method could not be used since the global perturbations affect all detector signals at the same time (a trick was used by Van der Hagen *et al.* to circumvent this problem, by artificially delaying signals)[4].
In BAR modeling, the two processes – upwards and downwards flowing signal disturbances, respectively – are assumed to be caused by two independent white noise sources. In addition, it is assumed that the signals of a specific detector at a specific discrete time instant, $n$, can be written as a linear weighted sum of earlier signal values of both detectors plus a white noise term:

$$\begin{aligned} \delta S_{1,n} &= \sum_{i=1}^{p} A_i S_{1,n-i} + \sum_{i=1}^{p} B_i S_{2,n-i} + w_{1,n}\,; \\ \delta S_{2,n} &= \sum_{i=1}^{p} C_i S_{1,n-i} + \sum_{i=1}^{p} D_i S_{2,n-i} + w_{2,n}\,. \end{aligned} \qquad (11)$$

The AR-coefficients $A_i$, $B_i$, $C_i$ and $D_i$ and the strength of the intrinsic white noise sources can be determined from the correlation functions of the time series, via the so-called Yule-Walker equations.[7] Usually, the model order, $p$, is determined from the Akaike criterion.[7] In our case, however, unusually large model orders turned out to be necessary to arrive at good results.
A graphical representation of a BAR-model is given in Fig. 8. The transfer functions of this

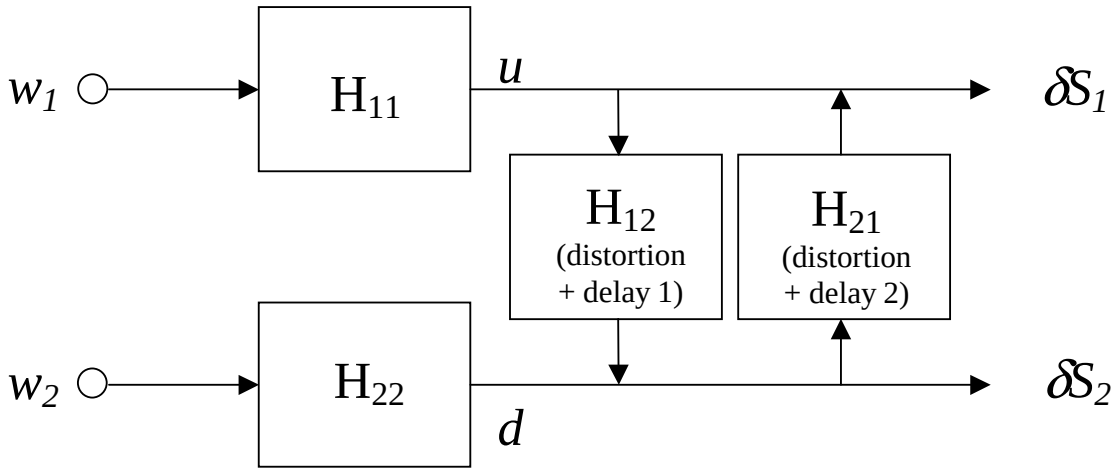


Figure 8. Scheme of a BAR model: two noise sources, $w_1$ and $w_2$, influence two detector signals.

scheme depend only on the AR-coefficients and contain – that is, for a successful BAR-model – all relevant physical information. Every physical noise source is modeled as the convolution of a hypothetical, so-called intrinsic, white noise source $w_i$ and a so-called shaping filter $H_{ii}$. (in fact, these physical sources correspond to the sources $u$ and $d$ from Eqs. (1)) The physical character of the noise source is imbedded in this shaping filter; the strength of the physical noise source is determined by both the strength of the intrinsic noise source $w$ and the modulus of the shaping filter. The measured noise signal $\delta S_i$ is composed by its own noise source plus that of the other signal via the transfer function $H_{ji}$. These transfer functions $H_{ji}$ contain the time delay and a possible distortion of the noise component between the two detector positions.

## 5. NUMERICAL SIMULATIONS

Numerical simulations were performed to study the potentials of BAR-modeling for the present purposes. To this end, two artificial noise series $\delta\hat{S}_{1,n}$ and $\delta\hat{S}_{2,n}$ were constructed based upon two uncorrelated white noise sources, with (discrete) delay 'times' $\tau_1=20$ samples and $\tau_2= 30$ samples:

$$\begin{aligned} \delta\hat{S}_{1,n} &= w_{1,n} + w_{2,n-\tau_2}\,; \\ \delta\hat{S}_{2,n} &= w_{1,n-\tau_1} + w_{2,n}\,. \end{aligned} \qquad (12)$$

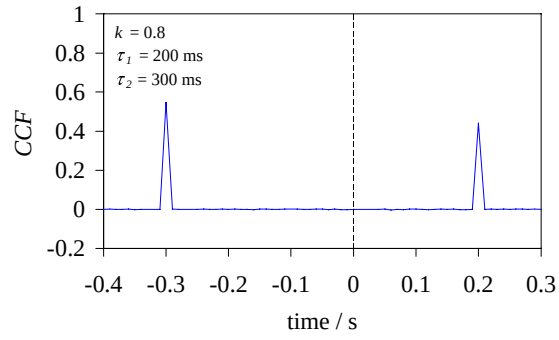


Figure 9. Characteristic functions calculated from simulated noise signals for $k$=0.8. *CCF* = cross-correlation function; *CPSD* = cross power spectral density; *NCR* = noise contribution ratio.

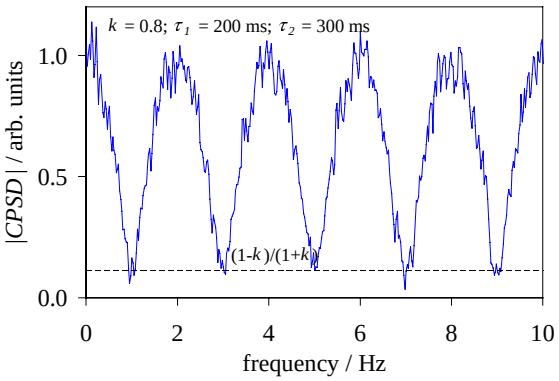


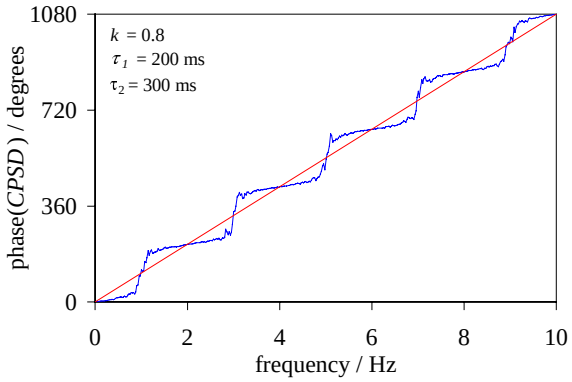


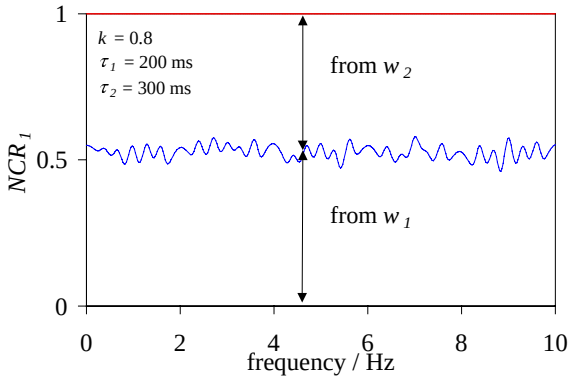


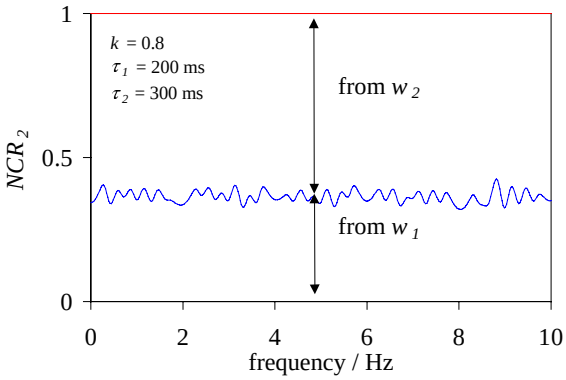


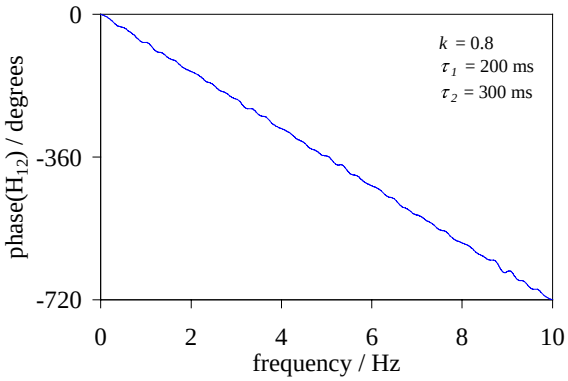


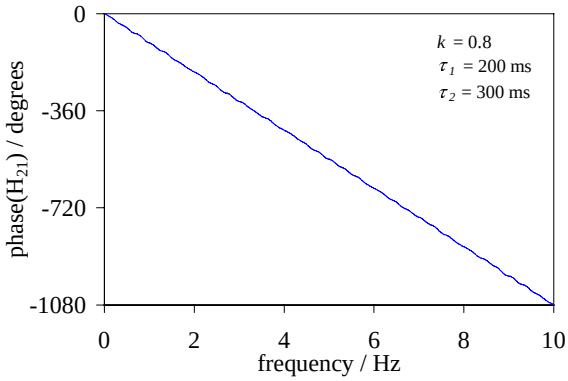

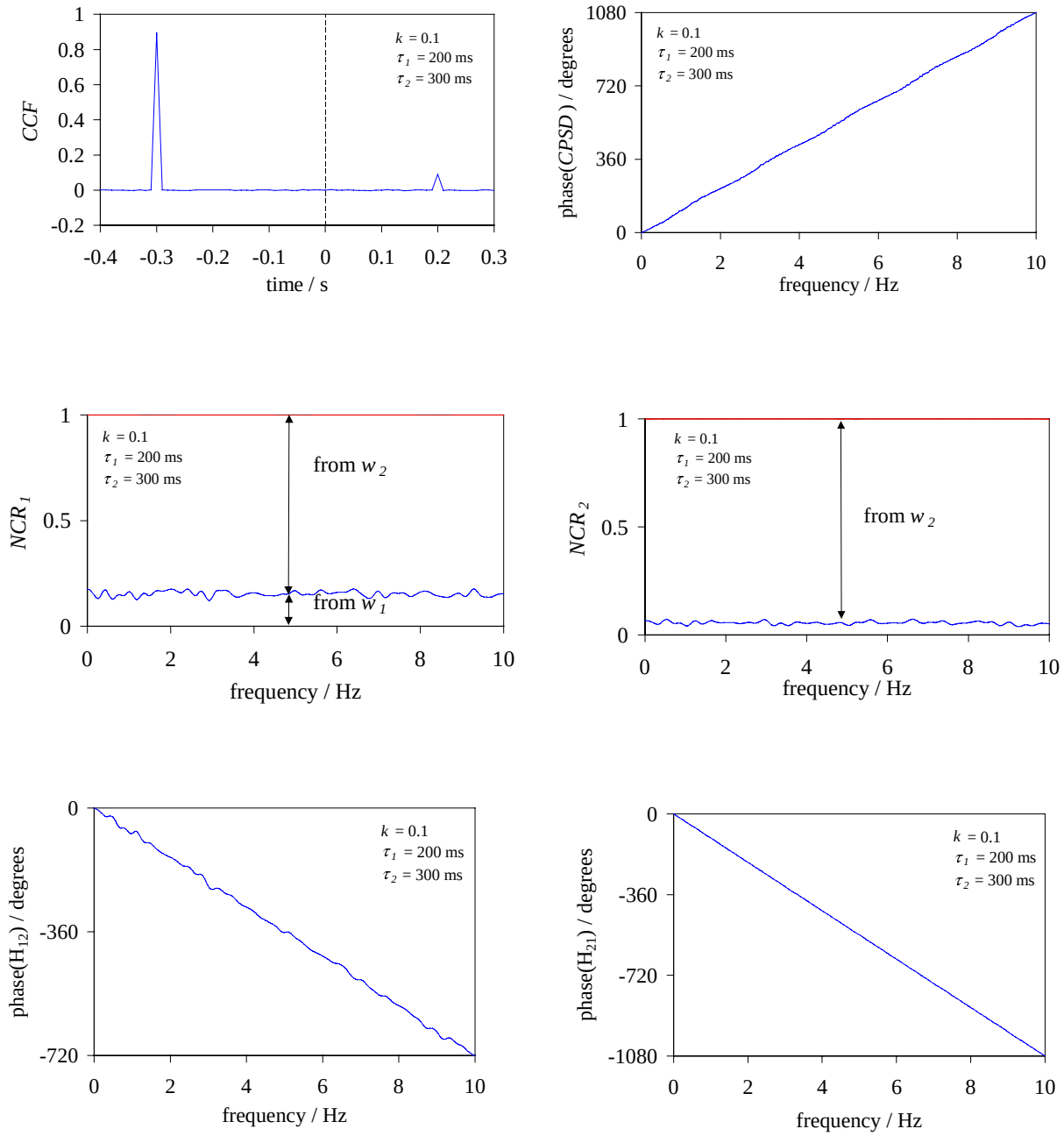


Figure 10. Characteristic functions calculated from simulated noise signals for $k$=0.1.
*CCF* = cross-correlation function;
*CPSD* = cross power spectral density;
*NCR* = noise contribution ratio.

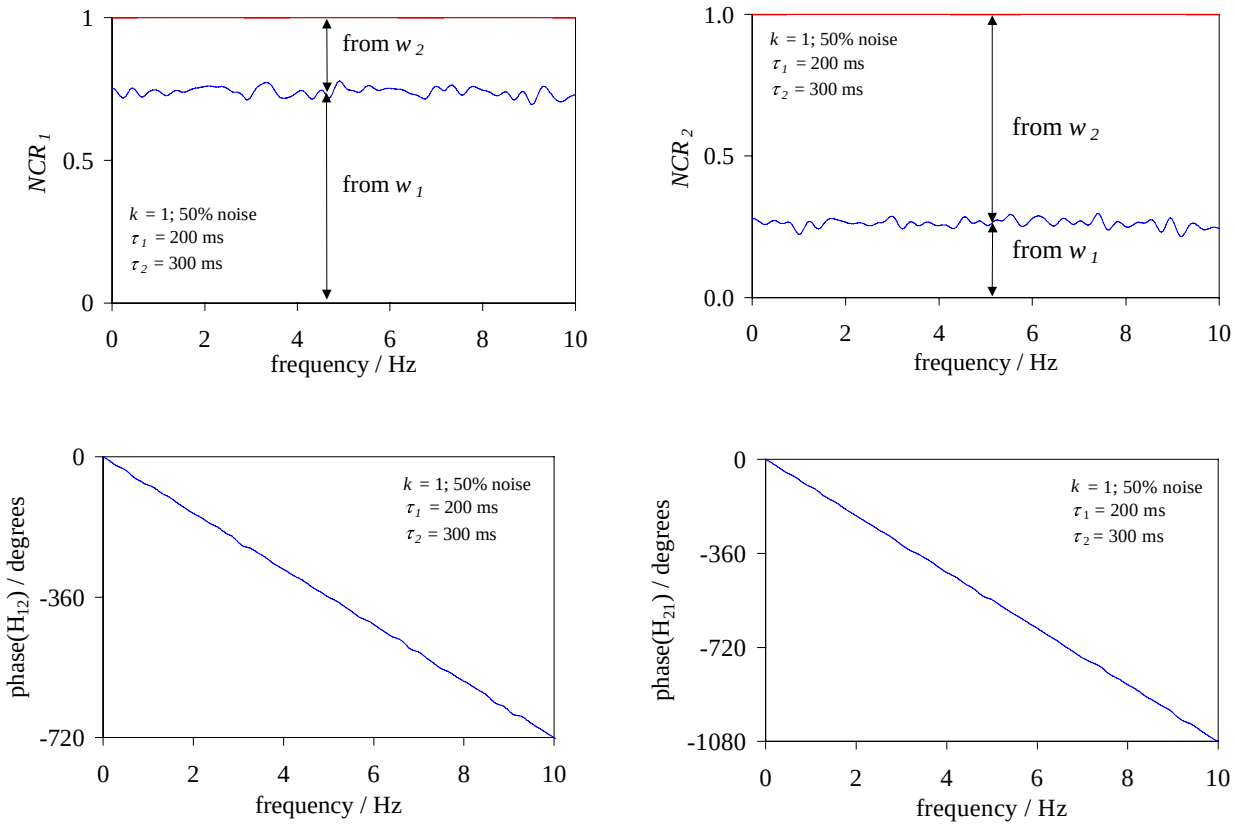


Figure 11. Characteristic functions calculated from simulated noise signals for $k$=1, with 50% parasitic noise added to both signals.
*CCF* = cross-correlation function;
*CPSD* = cross power spectral density;
*NCR* = noise contribution ratio.

The artificial sampling time was set to 10 ms. Each time series consisted of 512,000 samples, corresponding to a simulated measuring time of approximately 1.5 hours. The relative strength of the two noise sources was varied in order to test the performance at different $k$-values.
Figure 9 gives the results for a simulated system with *k=0.8* (the ratio of the variances of the two noise sources was taken equal to 0.8). The *CCF* and the modulus and phase of the *CPSD* of the simulated signals are presented in the top two three figures. The *CCF* has two clear maxima; one at –300 ms, the other at 200 ms, as expected. The maxima at -300 ms is larger, since noise source $w_2$ was stronger in this case. The *CPSD* modulus shows maxima and dips, in correspondence with Eqs. (6) and (10). Since the maxima of the CPSD have been normalized to unity, the minima are expected to have values of *(1-k)/(1+k)=0.111*, indicated by the dashed line. The phase spectrum (in blue) wags around the –300-ms slope (in red), with no distortion at f=1, 2, 3 … Hz, as expected.

The results of BAR-modeling are presented in the lower four figures. The first two figures present the so-called cumulative Noise Contribution Ratio (*NCR*), which is the composition of every measured signal broken down into the contribution of $w_1$ and that of $w_2$, as a function of frequency. Clearly, the power in $\delta\hat{S}_1$ comes for about 55% from $w_1$ (intrinsic) and for 45% from $w_2$. $\delta\hat{S}_2$ is for about 60% intrinsic ($w_2$) and for 40% due to $w_1$. Taking into account the *k*-value of 0.8, one would expect compositions for both signals as 45% $w_1$ and 55% $w_2$. Apparently, the exact separation of the moduli of the noise processes is rather difficult.
Next, the phase spectrum of the two transport processes (indicated as $H_{12}$ and $H_{21}$ in Fig. 8) are shown. Perfectly straight lines are the result; their slopes being perfectly in agreement with the delay times.

Figure 10 gives similar pictures for the case where one noise source is much weaker than the other, $k$=0.1. As can be seen from the phase slopes, the resulting estimated delay times are still perfect.

The artificial signals were distorted with 50% uncorrelated noise in a last example, where $k$=1. The *NCR*s clearly show the contribution of this extra noise term to the signals (Fig. 11): although noise sources $w_1$ and $w_2$ have equal strength, signal 1 is for 75% intrinsic: 50% is coming from the extra parasitic noise source; 25% is intrinsic (coming from $w_1$) and 25% comes from $w_2$, exactly as it should be. The slopes of the final phase spectra are again in excellent agreement with the artificial delay times.
Although these simulations do not cover the kaleidoscope of physical phenomena to be expected at 'real-life' experimental set-ups, they do give confidence in using BAR-modeling as an analysis tool.

## 6. EXPERIMENTAL RESULTS

Measurements where taken at the fluidized bed facility (shown in Fig. 1). The bed was filled with 1.89 mm polystyrene particles up to a height of 52 cm; the air flow rate used to fluidize the bed was 0.318 $m^3/s$, yielding a superficial air velocity of 3.1 m/s (which is equal to 43% of the terminal velocity). At such an air flow rate, the bed expands considerably. Although there is a clear radial and axial gas-fraction profile, one might say that the bed expands a factor two in height, yielding an average dilution of a factor two.[3]
Gamma-transmission measurements, each lasting 1 hour, were performed at two radial and two axial positions: radiating through the center of the bed and through the periphery (at a radial position $r/R_{set\text{-}up} = 0.77$), both at a low position in the bed (52 cm, from now on called 'bottom') and at a higher elevation (106 cm, from now on called 'top'). The two gamma beams and detectors were positioned 12 cm above each other (see Fig. 2).

Figures 12-15 present the characteristic functions – both from traditional correlation techniques and from BAR-modeling – for these four measurement cases. The order of the BAR-model was 100 for all cases. We will discuss the results one after the other.

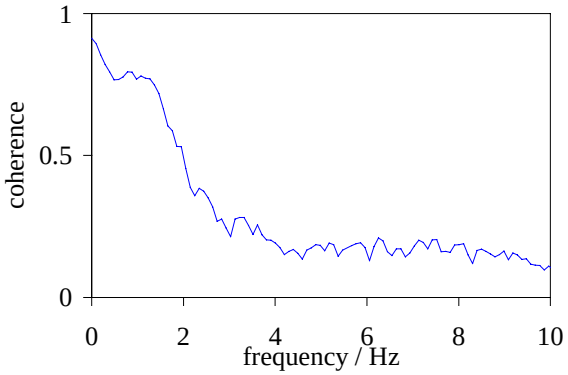


Figure 12. Characteristic functions calculated from measured gamma-transmission signals.
Measurement position:
**periphery** at the **top** of the bed.

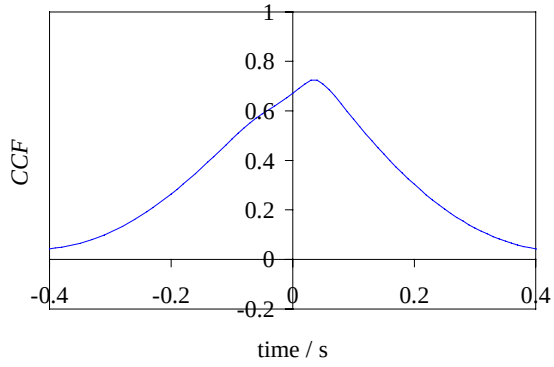


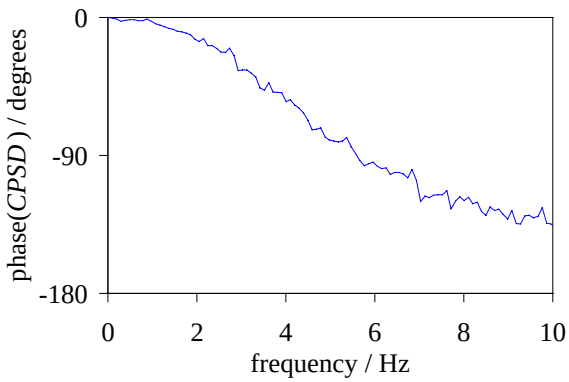


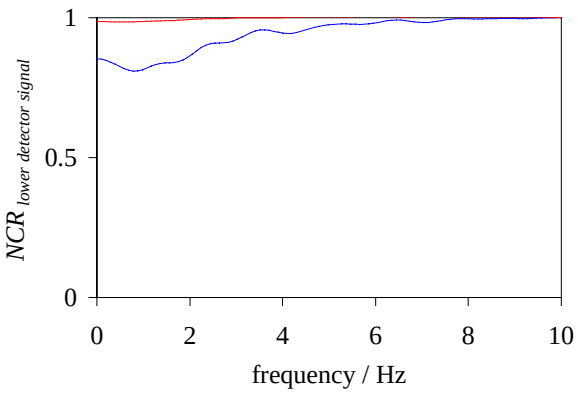


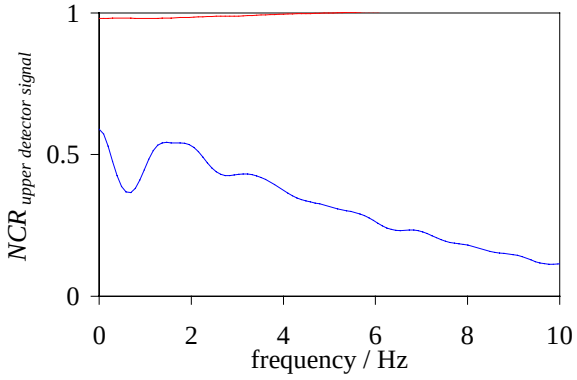


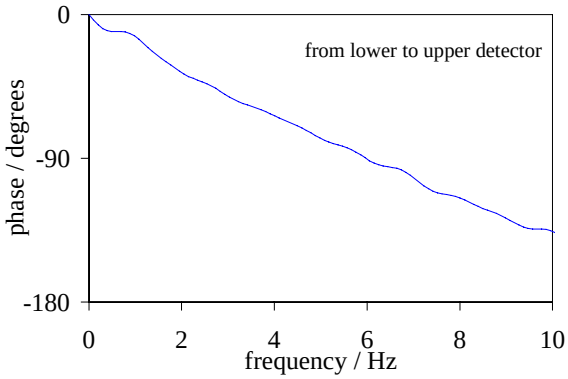


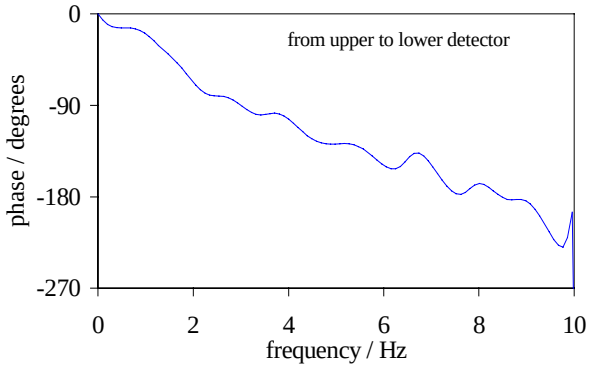

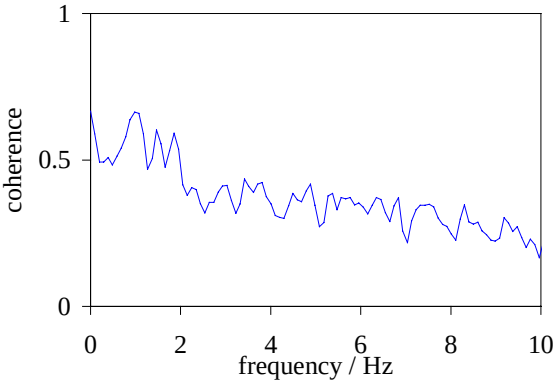


Figure 13. Characteristic functions calculated from measured gamma-transmission signals.
Measurement position:
**center** at the **top** of the bed.

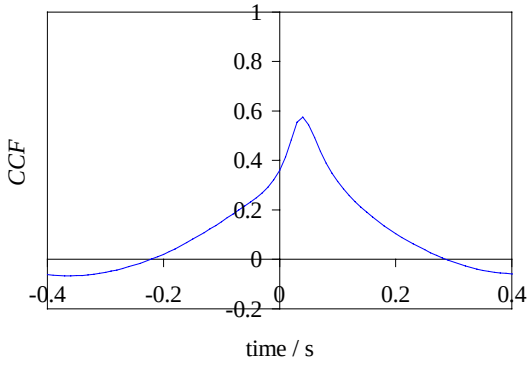


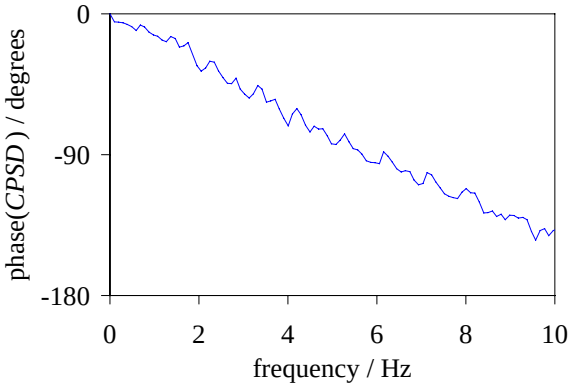


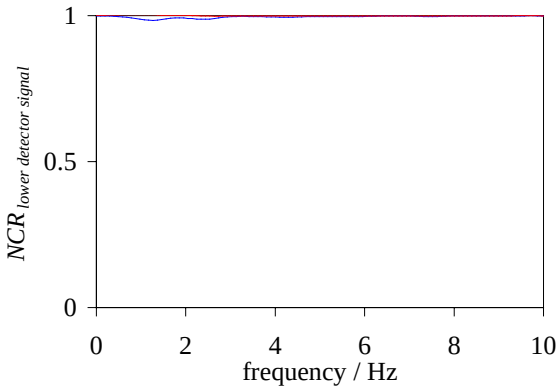


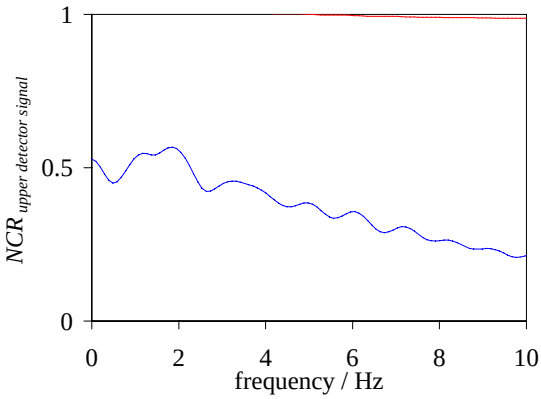


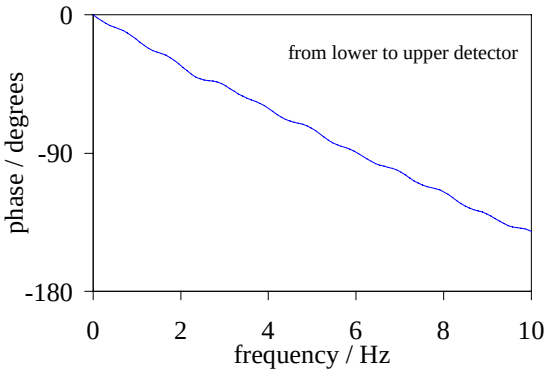


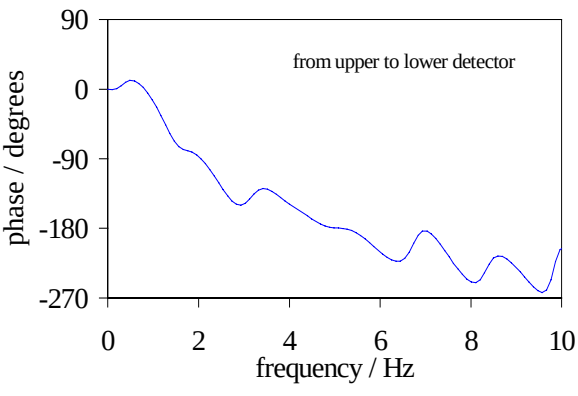

The results of radiating through the **periphery** at the **top** of the bed are displayed in Figs. 12. The two measured signals are strongly correlated for frequencies below 4 Hz, as can be seen from the coherence. The *CCF* shows a weak maximum around 35 ms; the phase of the *CPSD* of the measured signals is not straight, indicating the interference between the up-going noise and the down-going noise processes. BAR-modeling gives the separation of these processes. The *NCR* shows that the signal of the *lower* detector is at low frequencies for 80% composed by its own intrinsic noise source and contains some 20% noise that is coming from the other source. Fluctuations in the signal of the *upper* detector are for a considerable part due to the noise source of the lower detector (up to some 50% at 2 Hz), that have traveled upwards in the bed. The remaining part is intrinsic. The phase of the transfer function from lower noise source to upper detector signal ($H_{12}$ in Fig. 8) is fairly straight and corresponds to a delay time of 39 ms. Taking into account the detector separation of 12 cm, this gives a transport velocity of 3.1 m/s. The phase of $H_{21}$ (from upper source to lower detector) is not as straight, since the information traveling downwards is less strong. The phase slope gives a delay time of 65 ms (corresponding to a velocity of 1.9 m/s) for down-travelling processes.
This measurement leads to the conclusion that at the top of the bed density disturbances (particle clusters and voids) are travelling upwards and downwards at the bed periphery. The upward velocity is 3.1 m/s; the downward velocity is 1.9 m/s.

Figure 13 gives the results for the measurements at the **top** of the bed, radiating through the **center**. In this case, the gamma beams are influenced both by processes in the center of the bed and by processes in the periphery. However since, the gamma beam radiates for 77% of its length through the center, these processes will be dominating. The coherence shows the correlation between the two measured signals. The *CCF* shows a clear peak at 39 ms; the phase of the *CPSD* of the measured signals is rather straight, with a slope corresponding to 40 ms. The straightness of the phase indicates that the up-going noise process is strongly dominating ($k>>1$). BAR-modeling gives further evidence of this fact. The *NCR* shows that the signal of the *lower* detector is for 100% composed by its own intrinsic noise source (apart for some very tiny contribution around frequencies of 2 Hz). Fluctuations in the signal of the *upper* detector are for low frequencies for a considerable part due to the noise source of the lower detector, that have traveled upwards in the bed. The remaining part is intrinsic (local); apparently this part does not move downwards, or is strongly distorted during traveling, as it is not detected by the lower detector. The phase of the transfer function from lower noise source to upper detector signal ($H_{12}$ in Fig. 8) is perfectly straight, yielding a delay time of 40 ms, corresponding to a transport velocity of 3 m/s. The phase of $H_{21}$ (from upper source to lower detector) is strongly distorted, as one may expect, since no information is traveling downwards.
This measurement leads to the conclusion that at the top of the bed density disturbances (particle clusters and voids) are travelling upwards through the center, with a velocity of 3.0 m/s. The downward motion of the particles is to diffuse to be detected as clusters.

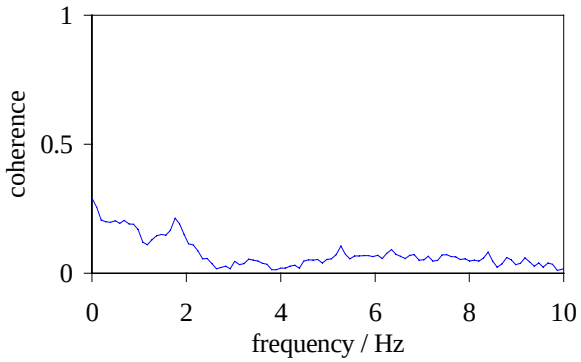


Figure 14. Characteristic functions calculated from measured gamma-transmission signals.
Measurement position:
**periphery** at the **bottom** of the bed.

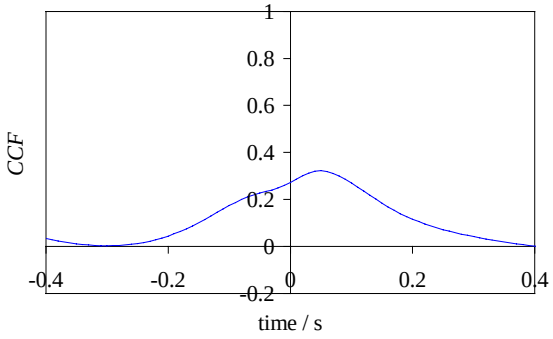


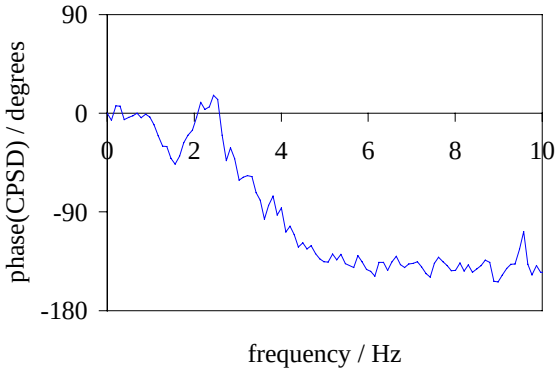


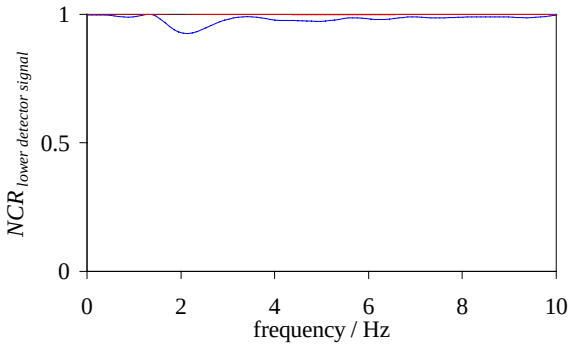


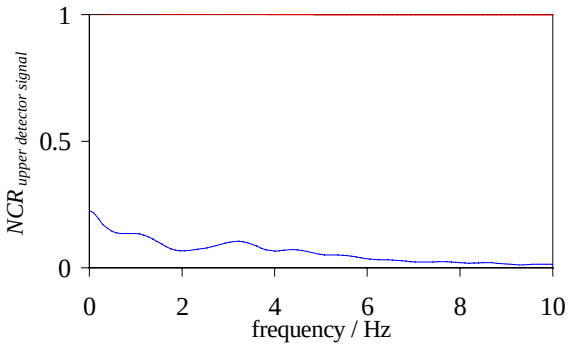


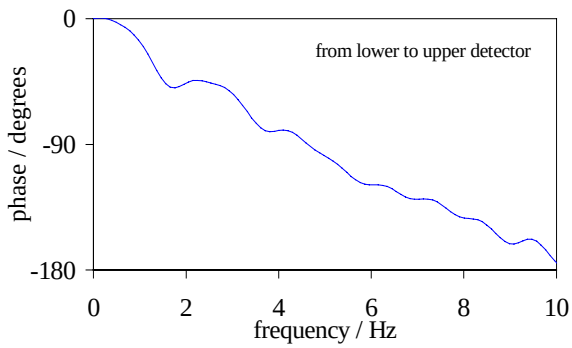


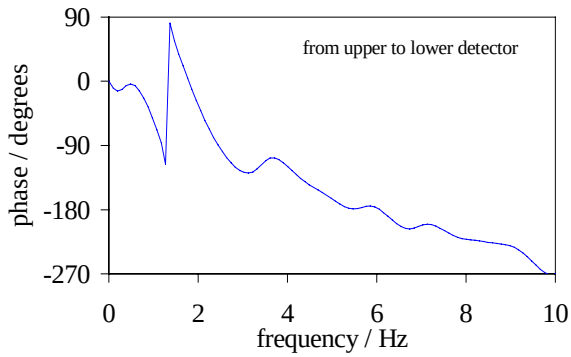

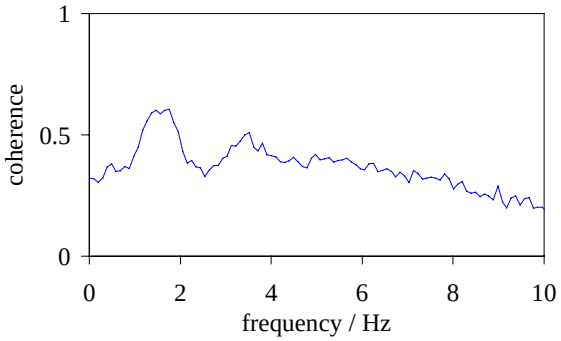


Figure 15. Characteristic functions calculated from measured gamma-transmission signals.
Measurement position:
**center** at the **bottom** of the bed.

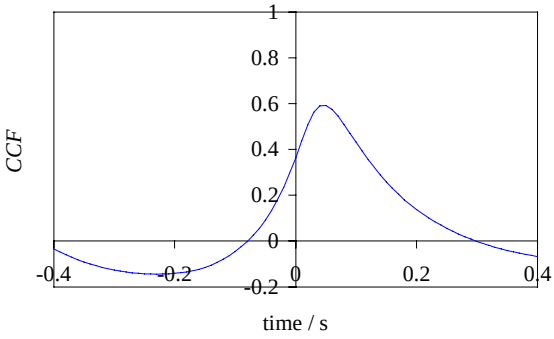


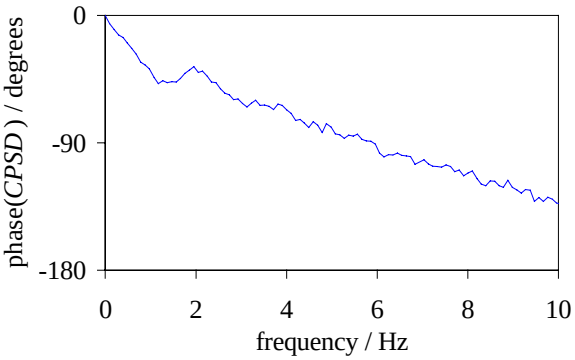


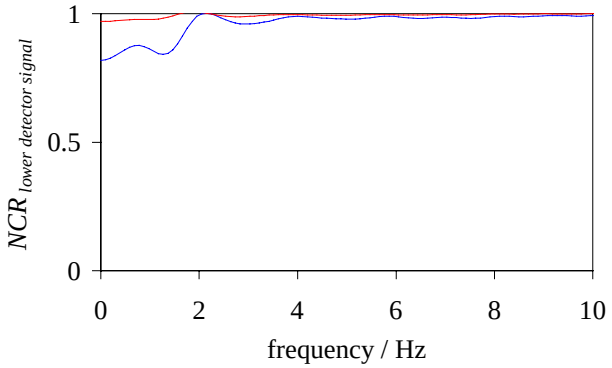


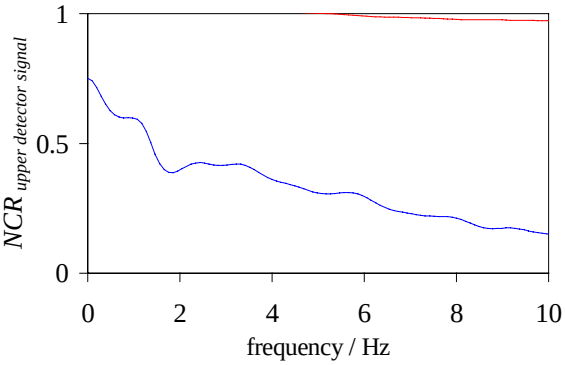


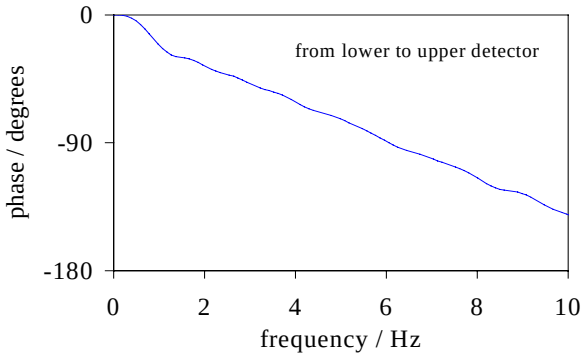


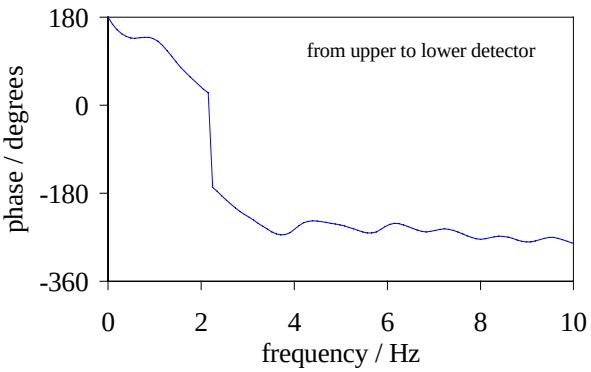

The results of radiating through the **periphery** at the **bottom** of the bed are displayed in Figs. 14. The two measured signals are weakly correlated, as is indicated by the coherence. The *CCF* shows a weak maximum around 49 ms; the phase of the *CPSD* of the measured signals is strongly distorted, possibly partly due to the low coherence. BAR-modeling shows that the signal of the *lower* detector contains only some minor components from the upper noise source (around 2 Hz). Fluctuations in the signal of the *upper* detector are for a small part due to the noise source of the lower detector. The fluctuations are mainly intrinsic. These *NCR*s are in agreement with the low coherence found. In spite of this weak signal correlation, BAR-modeling yields a fairly straight phase spectrum for the rising noise process. Its slope corresponds to a delay time of 51 ms, corresponding to a velocity of 2.4 m/s. The phase of $H_{21}$ is strongly distorted and does not lead to a clear transport phenomenon from upper to lower bed positions.
This measurement leads to the conclusion that at the periphery in the bottom of the bed, transport processes are not nicely structured; no clear up-ward and down-ward flowing processes can be distinguished. The upward velocity found is 2.4 m/s.

Finally, the results of radiating through the **bottom center** of the bed will be discussed (see Figs. 16). Here, a relatively strong correlation between the measured signals is found. Consequently, the *CCF* shows a clear maximum, around 46 ms. The *NCR* shows that the signal of the *lower* detector contains some 20% noise from the upper position at low frequencies. The signal of the *upper* detector is strongly influenced by the disturbances coming from below – up to some 70% at low frequencies. Due to this strong correlation, the phase of $H_{12}$ is fairly straight, yielding a delay time of 37 ms, corresponding to a transport velocity of 3.2 m/s. The phase of $H_{21}$ (from upper source to lower detector) is not straight at all, and starts off with a strange 180-degrees phase change, which would indicate an out-of-phase behavior of the two signals. This fact is not explained yet.
This measurement leads to the conclusion that at the bottom of the bed, density disturbances are traveling upwards through the center with a velocity of 3.2 m/s.

## CONCLUSIONS

The fluctuations of gamma-transmission signals, measured at a fluidized bed, can be explained from two physical phenomena: rising bubbles and particle clusters through the center of the bed and falling particles along the bed periphery.

An analytical model explains the specific features of the cross power spectral density (*CPSD*) of the signals of two axially displaced gamma-detector sets: the modulus of the *CPSD* shows maxima and minima and the phase shows a strong non-linear behavior. For simple systems, these features can be used to determine the rise and fall velocity of the particles.
In a physical bed however, the two processes are intertwined to such an extend, that a sophisticated analysis method has to be used. Bivariate autoregressive modeling (BAR) proved to be very useful. Numerical simulations were performed to indicate the strength of this method.
Applying BAR-analysis to the fluidized-bed measurements yielded a clear insight into the behavior of particle clusters. Rise velocities and speed of fall could be determined.

All in all, the method developed and presented here is another example of the usefulness of signal analysis for nuclear engineering research.

## REFERENCES


1. H. van Dam, T.H.J.J. van der Hagen, J.E. Hoogenboom, V.A. Khotylev and R.F. Mudde, "Statics and Dynamics of a Fluidized Bed Fission Reactor, Proceedings of ICENES'98, June 28-July 2, 1998, Tel-Aviv, Israel, pp. 609-616 (1998).

2. V.V. Golovko, J.L. Kloosterman, H. van Dam and T.H.J.J. van der Hagen, "Dynamic Core Stability Analysis of a Fluidized Bed Nuclear Reactor", PHYSOR 2000, May 7-11, 2000, Pittsburg, Pennsylvania, USA.

3. T.H.J.J. van der Hagen, W. Harteveld, R.F. Mudde and H. van Dam, "Gamma Transmission Measurements on Core Density Fluctuations of a Fluidized Bed Nuclear Reactor," Proceedings of IMORN 27, Valencia, Spain, November 18-20, 1997, pp. 157-164 (1999).

4. T.H.J.J. van der Hagen, I. Pázsit, O. Thomson and B. Melkerson, "Methods for the Determination of the In-phase and Out-of-phase Stability Characteristics of a Boiling Water Reactor," *Nuclear Technology*, **107,** pp. 193-214 (1994).

5. C.H. Knapp and G.C. Carter, "The Generalized Correlation Method for Estimation of Time Delay," *IEEE Trans. Acoust., Speech, Signal Processing*, **24(4)**, pp. 320-327 (1976).

6. R.F. Mudde, W.K. Harteveld, H.E.A. van den Akker, T.H.J.J. van der Hagen and H. van Dam, "Gamma Radiation Densitometry for Studying the Dynamics of Fluidized Beds," *Chem. Eng. Sci*. **54** (13/14), pp. 2047-2054 (1999).

7. M.B. Priestley, *Spectral Analysis and Time Series*, Academic Press, London, England (1994).

8. A.J.C. Stekelenburg and T.H.J.J. van der Hagen, "Two-Phase Flow Monitoring by Analysis of In-core Neutron Detector Noise Signals – a Literature Survey," *Annals of Nuclear Energy*, **20**, no. 9, pp. 611-621 (1993).